Monitoring atmospheric turbulence profiles with high vertical resolution using PML/PBL instrument

F. Blary, A. Ziad, J. Borgnino, Y. Fantéï-Caujolle, E. Aristidi and H. Lantéri.

Laboratoire J.L. Lagrange UMR 7293, Université de Nice Sophia-Antipolis/CNRS/OCA 06108 Parc Valrose Nice France

ABSTRACT

Wide-Field Adaptive Optics (WFAO) have been proposed for the next generation of telescopes. In order to be efficient, correction using WFAO require knowledge of atmospheric turbulence parameters. The structure constant of index-of-refraction fluctuations (C_N^2) being one of them. Indirect methods implemented in instruments as SCIDAR, MASS, SLODAR, CO-SLIDAR and MOSP have been proposed to measure $C_N^2(h)$ profile through different layers of the atmosphere. A new monitor called the Profiler of Moon Limb (PML) is presented. In this instrument, $C_N^2(h)$ profiles are retrieved from the transverse covariance via minimization of a maximum likelihood criterion under positivity constraint using an iterative gradient method. An other approach using a regularization method (RM) is also studied. Instrument errors are mainly related to the detection of the Moon limb position and are mostly due to photon noise. Numerical simulations have been used to evaluate the error on the extracted profile and its propagation from the detection to the inverse technique.

Keywords: atmospheric turbulence, site testing, instrumentation : adaptive optics & interferometry

1. INTRODUCTION

Wide-Field Adaptive Optics (WFAO) concepts are currently under development and have been proposed for the next generation of telescopes. WFAO are based the reconstruction of the volume of the atmosphere. In order to be efficient, correction using WFAO require knowledge of atmospheric turbulence parameters such as the profile of structure constant of air index-of-refraction fluctuations $C_N^2(h)$. A direct and accurate method for a $C_N^2(h)$ profile measurement is the exploitation of radio-sounding balloons[1] . However, due to their expensiveness (loss of the balloon in the environment) and the delay between each layer acquisition (around 2h of ascent time), other indirect methods such as the MASS, SLODAR, CO-SLIDAR and MOSP have been proposed. These methods use Angle of Arrival (AA) fluctuations and/or scintillation of stars in order to extract atmospheric turbulence parameters.

The indirect $C_N^2(h)$ profile measurement require an inverse problem resolution with a positivity constraint due to the refractive index nature. Inverse problem resolution using variable change[2] or non-negative least square algorithm[3 4] were exploited. For non-linear equations resolution, specific algorithms such as simulated annealing[5 6] were also used for $C_N^2(h)$ profile extraction.

The Profiler of Moon Limb (PML) initially known as "Profileur Bord Lunaire (PBL)" has been developed for the extraction of the $C_N^2(h)$ profile with high vertical resolution. The instrument uses lunar limbs fluctuations as an equivalent of a double star continuum. The observation of an extended object give us the possibility to size up a broad field of angular separation, allowing us to scan the whole atmosphere with multiple layers.

In this paper, a brief summary describing the PML components is given. The theoretical background of the extraction of $C_N^2(h)$ profile from PML measurements and their approximations are presented. Emphasis is made on the inversion techniques used for $C_N^2(h)$ profiles extraction. Comparison of $C_N^2(h)$ profile results between Maximum Likelihood criterion and a regularization method are discussed. The PML instrument was installed on different sites and results obtained in the Dome C campaign are shown. Instrument error are mainly related to the detection of the Moon limb position and are mostly due to photon noise. The propagation of the noise from the detection to the extracted profile have been studied, leading to the error bars of the measured $C_N^2(h)$ distribution.

Figure 1. PML telescope front side with the implemented two sub-apertures mask. Pupils diameter D = 6cm, baseline B = 26.7cm.

Figure 2. The PML instrument backside with the collimating and imaging lens, the Dove prism and the CCD camera.

2. PML INSTRUMENT

The PML operating method is based on the Differential Image Motion Monitor (DIMM)[7] with the observation of an extended object instead of a single star. In our case, Moon and Sun limbs were used as extended object to retrieve atmospheric turbulence parameters. The PML itself consists of a 16-inch telescope with a pupil mask composed of two sub-apertures mounted at the entrance pupil (figure 1). The pupils have a diameter D = 6 cm and are separated by a baseline B= 26.7 cm . The two beams of each sub-aperture are separated with a lens placed at the focal length from the telescope focus. The image of one of the beam is reversed by the use of a Dove prism and both images are reformed using a second lens. (figure 3)

The two images of the moon limb are recorded by a PCO PixelFly CCD camera installed on an automatic micro control plate controlled by software (figure 3). Each optical element is also placed on a Micro-control plate for fine adjustments. Exposure time of the CCD camera is set to 5 ms on a 640 x 480 pixel matrix with a 9.9 x 9.9 µm pixel size. The spectral response of the camera is maximum for $\lambda = 0.5$ µm in a 375-550 µm range

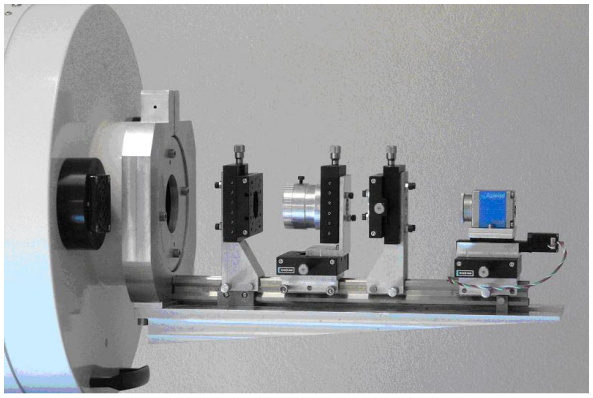

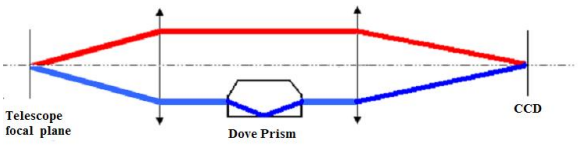

Figure 3. The PML instrument optical device composed of a Dove prism placed between collimating & imaging lenses. The role of the Dove prism is to reverse one of two images obtained with the sub-pupils.

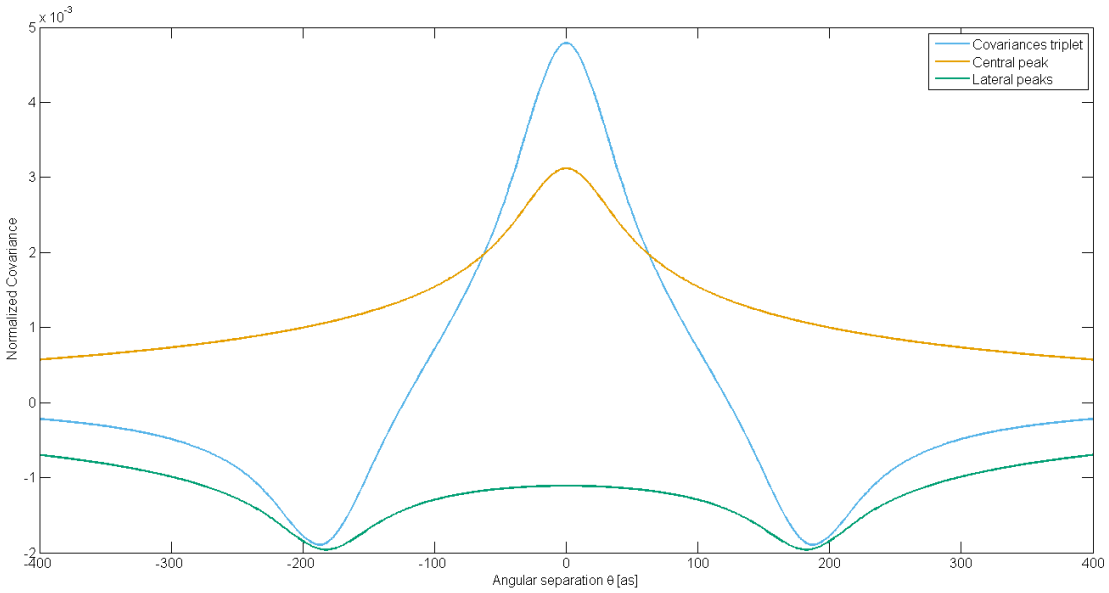

Figure 4. Normalized covariance triplet of a turbulent layer at an altitude h=300m with a baseline B=26.7cm. The central peak is always positive whereas both lateral peaks, centred at $\theta h = -B$ and $\theta h = B$, are negatives.

3. THEORETICAL BACKGROUND

The transverse covariance of AA fluctuation (α) difference between two images of the Moon limb as shown in figure 4 (one for each pupils) perpendicular to the baseline is equal to :

$$C_{\Delta\alpha}(\theta) =< [\alpha(r,\theta_0) - \alpha(r+B,\theta_0)][\alpha(r,\theta_0+\theta) - \alpha(r+B,\theta_0+\theta)] > \tag{1}$$

where B = 26,7 cm is the baseline between the sub-apertures, θ is the angular separation along the limb, θ_0 is assumed equal to zero and brackets <> stand for spatial average over r. Developing this previous equation give us :

$$\begin{aligned} C_{\Delta\alpha}(\theta) =& < \alpha(r,\theta_0)\alpha(r,\theta_0+\theta) > + < \alpha(r+B,\theta_0)\alpha(r+B,\theta_0+\theta) > \\ & - < \alpha(r,\theta_0)\alpha(r+B,\theta_0+\theta) > - < \alpha(r+B,\theta_0)\alpha(r,\theta_0+\theta) > \end{aligned} \tag{2}$$

For a turbulent layer at an altitude h, the angular separation θ correspond to a spatial separation as $\rho = \theta h$. Based on this assumption, eq.2 can be written in terms of spatial covariance as :

$$C_{\Delta\alpha}(\theta) = \int_0^\infty dh C_N^2(h) K(B,\theta,h) \tag{3}$$

where $K(B,\theta,h)$ is a normalized covariance triplet equal to :

$$K(B,\theta,h) = 2C_\alpha(\theta h) - C_\alpha(B-\theta h) - C_\alpha(B+\theta h) \tag{4}$$

and $C_\alpha(\rho)$ is a normalized spatial covariance of AA fluctuations given by Avila and al.[8] :

$$C_\alpha(\rho) = 1.19 sec(\zeta) \int_0^\infty df\, f^3 (f^2+f_0^2)^{-11/6}\ [J_0(2\pi f\rho) + J_2(2\pi f\rho)] \left[2\frac{J_1\pi Df}{\pi Df}\right]^2 \tag{5}$$

where D is the sub-aperture diameter, f is the modulus of the spatial frequency, $f_0 = \frac{1}{L_0}$ is the inverse of the outer scale and ζ is the zenith distance.

The whole atmosphere is the integration of multiple layers. Thus the covariance triplet shown in eq.4 is defined for each layer. This triplet is composed of a central peak and two lateral peaks centred at θh_i where h_i is the i^{th}-layer altitude. Central covariance can be obtained directly from one of the two moon limbs. Thus, subtraction of $2C_\alpha(\theta h)$ from the triplet lead directly to the lateral peaks $-[C_\alpha(B-\theta h)+C_\alpha(B+\theta h)]$.

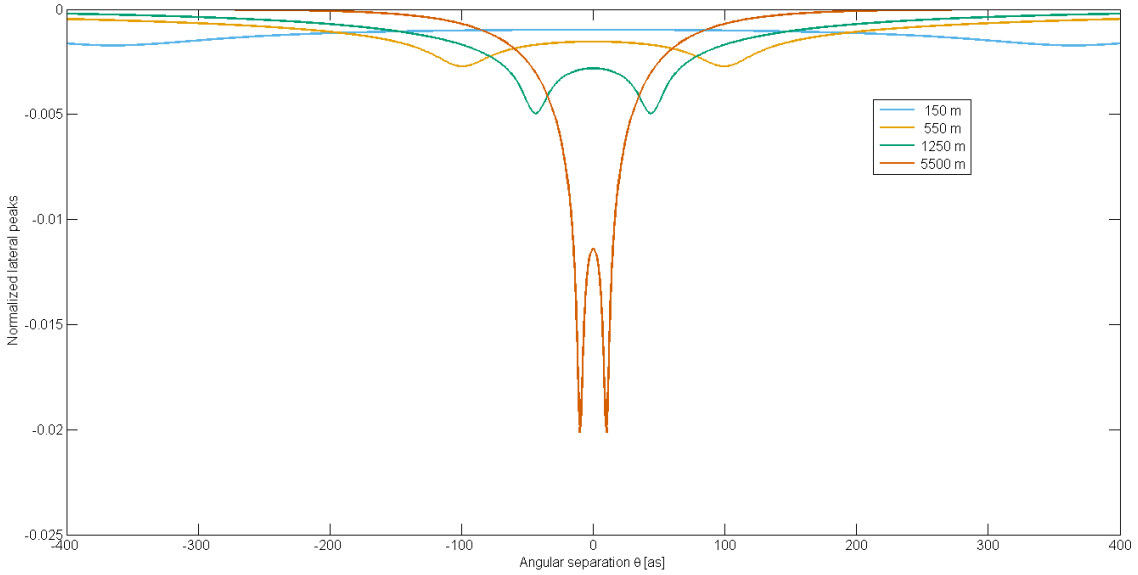

Figure 5. Normalized lateral covariances for multiple layers (150,550,1250 and 5500 meter) with the same baseline $B = 26.7$cm. The covariance thickness is dependant of the layer altitude.

An example of a covariance triplet at h=300m is shown in fig 4. Multiple lateral peaks for different altitude are shown in figure 5. We can see in these figures the influence of the baseline B on the lateral peaks minima positions ($B = \theta h$). One can also see that higher the layer is in altitude, thinner the covariance is.

Eq. 5 is non-linear but analytical solution of the integral expression has been made by Conan[9] through the use of Mellin transform. Resulting covariances are simplified into series or finite solutions. Approximations however are different depending on the baseline length. We used these approximations and the assumption of a discrete turbulent profile to transform eq. 3 into

$$C_{\Delta\alpha}(\theta) = \sum_{i=0}^{h_{max}} \Delta h_i C_N^2(h_i) \widehat{K_\alpha}(B, h_i, \theta) \tag{6}$$

where $\widehat{K_\alpha}(B, h_i, \theta)$ is the modified spatial covariance triplet and Δh_i is the thickness of the layer i. Eq. 6 is equivalent to a matrix form : $Y = M.X$ where X and Y are both vectors corresponding respectively to the sampled $C_N^2(h_i)$ and the covariance difference $C_{\Delta\alpha}(\theta_j)$, the matrix M contain the modified spatial covariance triplet weighted with Δh_i : $M = \widehat{K_\alpha}(B, h_i, \theta_j).\Delta h_i$.

As explained previously, both central and lateral peaks can be separated from the global covariance. Moreover, the covariance difference vector Y and the modified spatial covariance matrix M can be altered in order to exploit parts of the covariance triplet. In our case we used only lateral peaks by applying the difference $[K_\alpha(B, h_i, \theta_j) - 2C_\alpha(\theta_j, h_i)]$ in order to retrieve the $C_N^2(h_i)$ profile.

4. DATA PROCESSING

For each acquisition sequence of 1 minwith a number N ($N = 1000$) raw images are processed firstly by a flat and dark field correction on each image. A 3x3 pixel block median filter is then applied in order to slighty blur them, remove the small features of the moon limb and partially remove Poisson noise. Each image is then separated into two parts containing the moon limb of each aperture. The edge itself is retrieved by convolution of the resulting image with a 3x3 Prewitt edge detector. Centroid on each column are then calculated. Since a small angle between the Top and Bottom induced by the Dove Prism can remain, correction is made by slightly rotating the set of 1000 images (rotation correction being inferior to 1°) in order to fit both Top and Bottom edges. Moon drift between each image is also corrected in the same manner using the largest features of the moon as references. Finally, edges containing incoherent data are withdrawn of the 1000 data-set so as to avoid error propagation on upcoming covariance calculation.

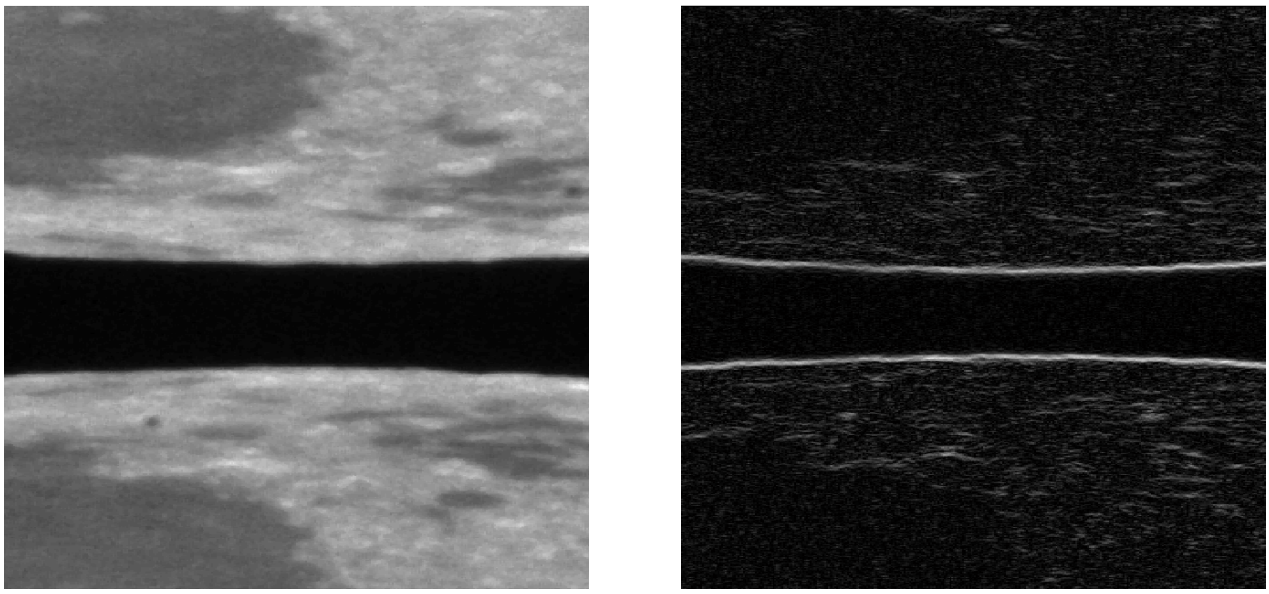

Figure 6. PML Moon Limbs acquisition before and after correction (flat and dark field, median filtering) and Prewitt edge detector convolution. Centroid calculation is used along the Moon Limbs to retrieve edge position.

The covariance of AA fluctuation difference $C_{\Delta\alpha}(\theta)$ between the two moon limbs is deduced after the above processing. Calculating differential covariance for each image have the advantage of being insensitive to vibration effects. Two estimations of the central covariance $C_\alpha(\theta)$ integrated over the whole atmosphere are calculated using the Top and Bottom edges separately. The central covariance is then subtracted, leading to lateral covariances which are used for $C_N^2(h)$ profile estimation. Angular separation covariances are obtained for each pixel along the 640 pixels of the CCD camera (each pixel corresponds to $\sim 0.57''$). Some of the 640 pixels and N images are withdrawn due to the Moon drift correction and incoherent data suppression.

5. INVERSE PROBLEM RESOLUTION

As seen in eq. 6 , the relation between the vector X containing the $C_N^2(h)$ profile and the measured covariance Y is linear. However, due to the approximation made on the covariance triplet, the matrix M is ill-conditioned. The condition number $\kappa(M) = ||M||||M^{-1}||$, translating the error propagation induced by M, is of the order of 10^5. Thus, direct resolutions of the equation system are avoided. A least square method using the initial criterion $J(X) = ||Y - MX||^2$ is used instead in order to retrieve the best estimation of X. The possibility of having negative refractive index using analytical solution of the least square method make the direct resolution inaccurate. To take into account the positivity constraint imposed by the $C_N^2(h)$ profile nature, other approach were exploited. An iterative gradient method under positivity constraint[10] was firstly used for the mean square criterion $J(X)$ minimization.

The algorithm start by calculating the gradient of $J(X)$ equal to $\Delta J(X) = 2M^T(MX - Y)$ where M^T is the transposed matrix of M and $\Delta J(X)$ will be the descent direction. The stepsize α is inserted in the algorithm and is computed at each iteration to ensure the convergence of the algorithm. Thus, for each k iteration, the new array X_k is equal to :

$$X_k = X_{k-1} - 2\alpha M^T(MX_{k-1} - Y) \tag{7}$$

The positivity constraint is applied at the end of each iteration by projecting all negative elements of the solution array X on a positive constant . This constant is arbitrary and must have a value equal or above 0. The algorithm is stopped when the relative error $\epsilon = \frac{|J(X_k) - J(X_{k-1})|}{|J(X_{k-1})|}$ between two k-iteration is equal to or below an imposed threshold. The algorithm also stop if ϵ is not reached before a defined number of iteration. Another approach, using the estimation of square root of the refractive index $\sqrt{C_N^2(h)}$ instead of the negative elements projection was also studied. However, due to the matrix size and condition number, finding the best estimation of $\sqrt{C_N^2(h)}$ using iterative algorithm is slow, making it hard to converge to an optimal solution.

The integrated $C_N^2(h)$ profile from the inversion is compared to the integrated $C_N^2(h)$ profile of the whole atmosphere using the Fried parameter r_0 ($r_0^{-5/3} = 16.7\lambda^{-2}\int dh C_N^2(h)$)[11] previously calculated with the DIMM[7] method. The residual energy is considered to be the $C_N^2(h_0)$ of the lowest part of the ground layer ($h < 100$m).

Since the measured covariance is an average of 1000 acquisition and measurement error is assumed, a mean square solution would be influenced by statistical errors and noise. Thus, the initial criterion was modified by a maximum likelihood one : $J(X) = (Y - MX)^T C^{-1}(Y - MX)$ where C is a diagonal matrix with Y variances σ_Y^2. The addition of a weighting matrix does not change the algorithm itself. The gradient in eq.7 is simply rewritten as :

$$X_k = X_{k-1} - 2\alpha M^T C^{-1}(MX_{k-1} - Y) \tag{8}$$

Based on the hypothesis that the structure constant $C_N^2(h)$ profile is steady, a regularization method was also used, in this method we add a penalty term $J_{RM}(X) = \beta||\nabla X||^2$ to the measurement fidelity criterion $J_(X)$. The regularization factor β allows a trade-off between $J(X)$ and $J_{RM}(X)$. Such a regularization gives the possibility to smooth the $C_N^2(h)$ profile for better coherence and thereby avoid compensation of two neighbouring layers. The final criterion $J(X)$ is therefore equal to :

$$J(X) = (Y - MX)^T C^{-1}(Y - MX) + \beta||\nabla X||^2 \tag{9}$$

6. PML FIRST RESULTS AND ERROR ANALYSIS

The PML instrument was first installed at the Dome C site in Antarctica for the whole year 2011. Radio-sounding balloons were employed on the same site, giving the possibility to compare PML results with a median profile. Fig.7 shows $C_N^2(h)$ profile obtained at Dome C on January 25^{th}, 2011 at 16h45 UT while the measured covariance

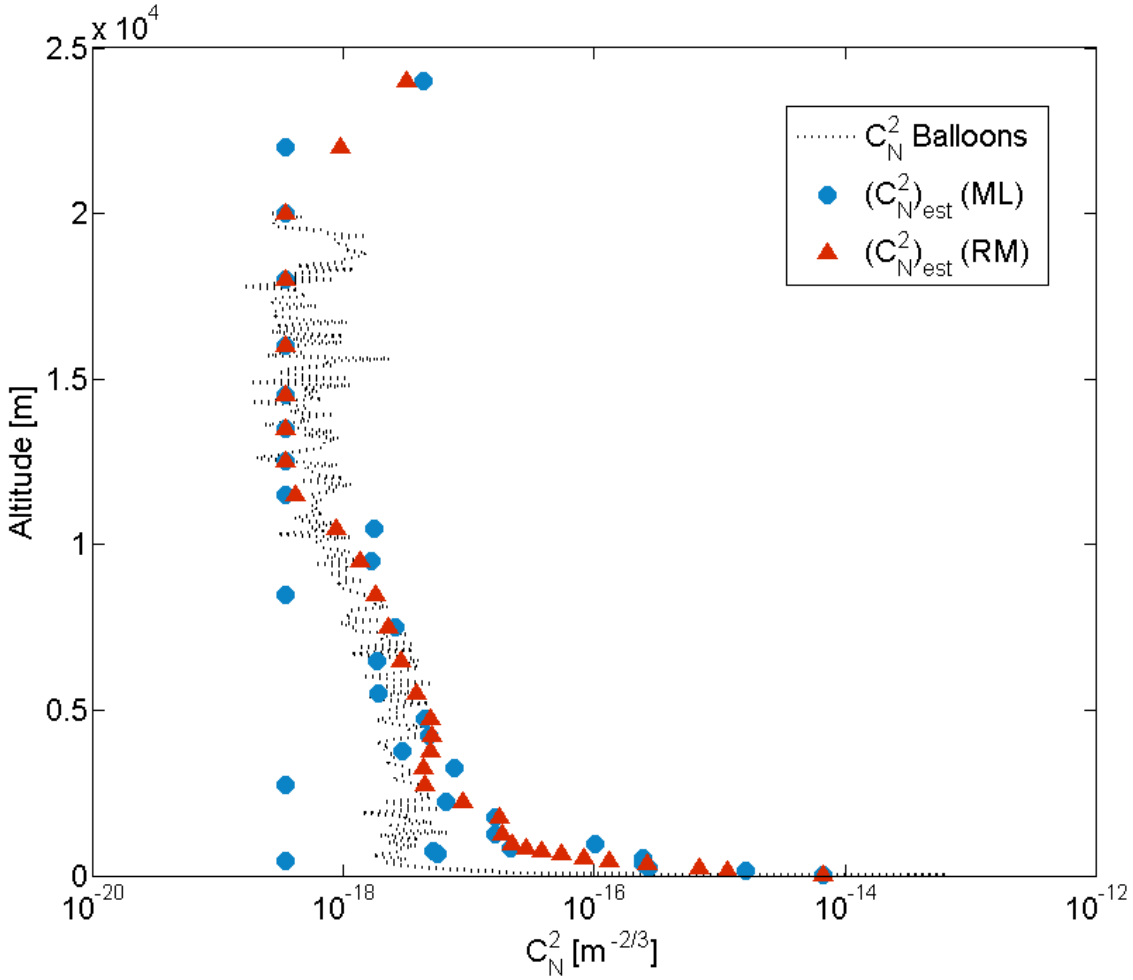

Figure 7. $C_N^2(h)$ Profiles from PML at Dome C (Antarctica) on January $25^t h$, 2011, at 16h45 UT. Both ML and RM minimization algorithms were used. The regularization of the regularization method giving a smoother profile than the ML one. The RM algorithm is also less sensible to error, mostly due to a better structure in the lower layers of the atmosphere.

and its estimation for the same time are shown in fig.8. The estimated Fried parameter deduced from the 16h45 UT profile was equal to $r_0 = 8.2$cm while the median balloon from the 2005 campaign leads to $r_0 = 6.7$cm.

For this profile extraction, both ML and ML+RM criterion were used. The non-negative projection was set to $10^{-18}m^{-2/3}$ and the RM β constant was equal to 0.3. The ML minimization is able to fit measured data correctly while avoiding most of the noise contribution. The resulting profile is similar to the Radio-sounding balloons profile with a few incoherent $C_N^2(h)$ layers. These latter instabilities are mostly due to a poor refractive index allocation between adjacent layers. The ML+RM minimization add a constraint on this refractive index attribution and smooth the $C_N^2(h)$ profile for better coherence. This regularization is more visible on the low altitude layers where fluctuations between two adjacent layers using the initial ML criterion can go beyond $100m^{-2/3}$. Nonetheless, the use of a constant β in the RM criterion impose an arbitrary constraint on the profile extraction. Thus, a well choice of β constant have to be done in order to avoid biased $C_N^2(h)$ profile.

Error sources on the PML monitor are related to the detection of the Moon Limb position. Similary to the MOSP instrument, photon noise and detector noise are the main contributor to the error on the $C_N^2(h)$ profile.[6] Simulated Moon limb image using a 2D Heaviside function on which seeing condition and aperture transfer

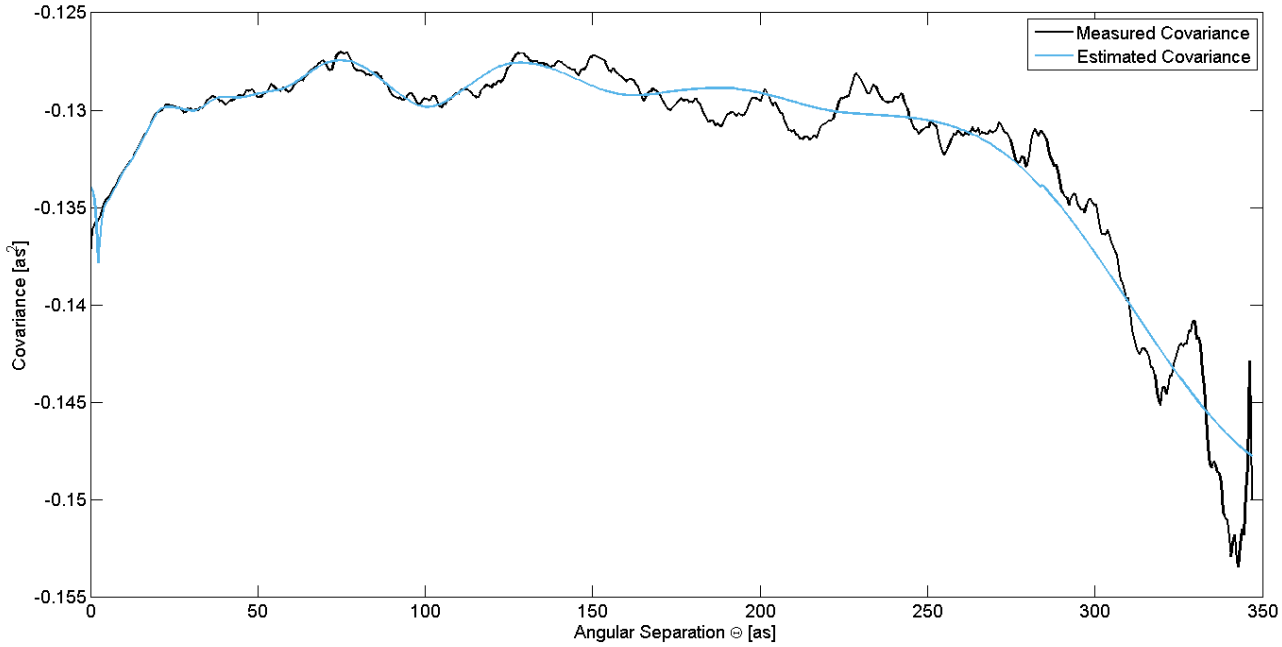

Figure 8. measured and estimated lateral covariances obtained with PML at Dome C (Antarctica) on January 25^{th}, 2011 at 16h45 UT.

function are added by convolution were created using a previous method[6] . Poisson noise were added on the artificial images in order to simulate the photon error contribution. Covariances of simulated Moon limbs are then extracted with the same number of N=1000 samples. The estimated error on the lateral covariance due to the photon noise is at maximum 0.5% in the conditions of the results presented in fig 7.

The error propagation into the inverse problem resolution algorithm is done by adding the propagated covariance error in a theoretical covariance using a $C_N^2(h)$ profile similar to experimental results (in our case a profile similar to the median radio sounding balloon profile obtained in Dome C). The error criterion for estimated $C_N^2(h)$ profile is equal to :

$$\epsilon_{PH} = \sum \frac{|C_N^2(h)_{est} - C_N^2(h)_{ref}|}{C_N^2(h)_{ref}} \tag{10}$$

where $C_N^2(h)_{ref}$ is the profile used for the theoretical covariance construction and $C_N^2(h)_{est}$ is the estimated profile after minimization.

A serie of 100 simulation were run using the mean propagated covariances of 10 acquisitions set with photon noise. In the case of the maximum likelihood, the mean error ϵ_{PH} is equal to 3.75% while the expectation maximization for the same serie gave us an error of $\epsilon_{PH} = 2.25\%$.

As an example, an estimated profile obtained after inversion of a theoretical covariance using simulated images is shown in figure 9. Both method used for the inversion technique show a good fidelity to the true profile. The RM criterion however give a better fidelity by improving the refractive index allocation between neighbours. Influence of the regularization method is more visible on the lower layers where the distances between each of the latter are the shortest and. Consequently, the additional constraint imposed by the RM criterion amplify the sturdiness of the algorithm to photon noise and thus explain the better ϵ_{PH} obtained using ML+RM algorithm.

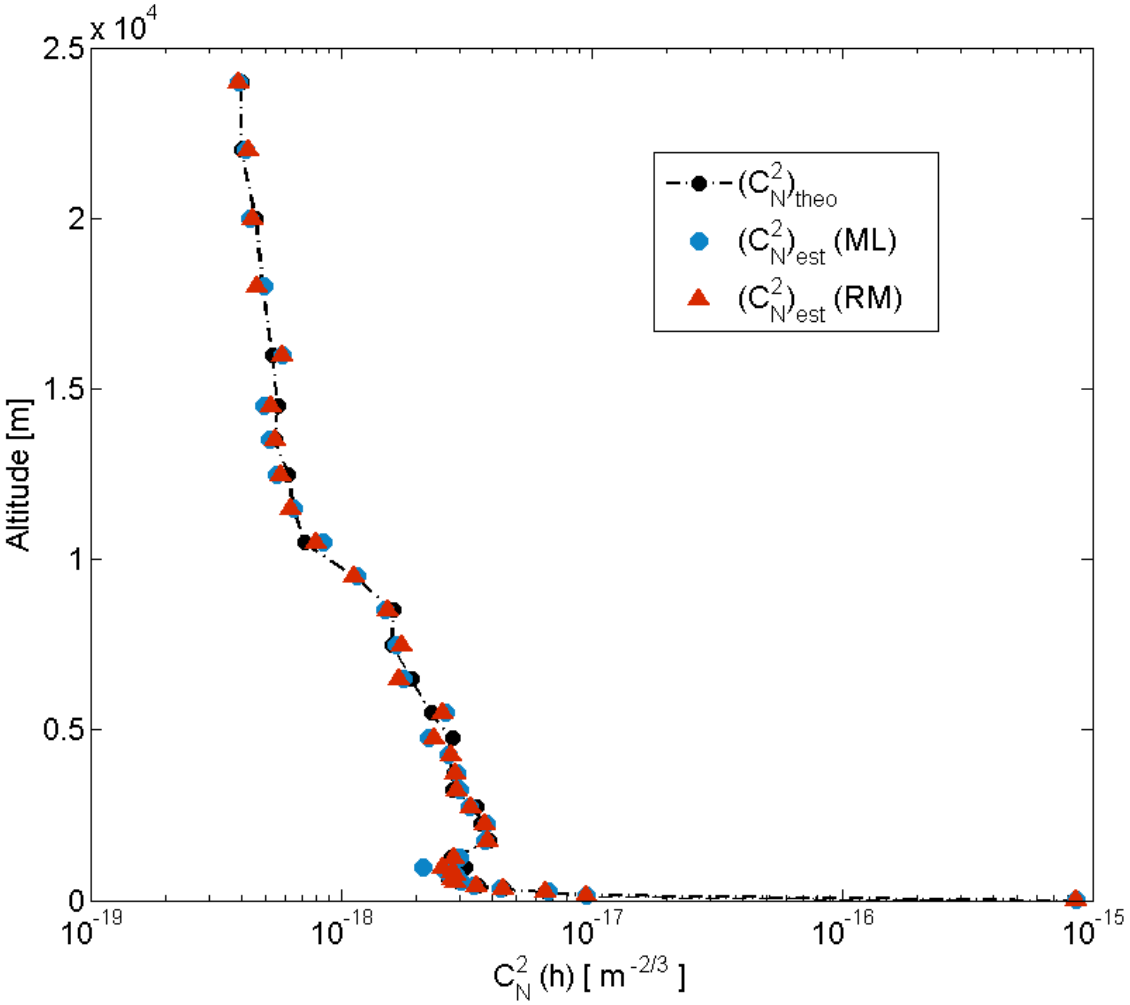

Figure 9. $C_N^2(h)$ Profiles estimation based on theoretical covariance using simulated Moon Limbs images with Poisson noise addition.

7. CONCLUSION

The PML instrument is able to give the $C_N^2(h)$ profile with high vertical resolution with an induced photon noise error on the estimated profile below 5%. Other parameters of the turbulence can also be measured : Outer Scale profile $L_0(h)$ estimation were already made using simulated annealing.[6] Moreover, Isoplanatic and Isopistonic domains can also be determined using the PML instrument[12] .

One aim of the PML instrument is to minimize the delay between Moon Limbs acquisition and $C_N^2(h)$ profile extraction. To do so, real time mechanical adjustment of the instrument is studied in order to reduce numerical post-processing corrections. Optimization of image acquisition, data processing and inverse problem resolution algorithms are also on the way. Further improvement of the inverse problem resolution are also considered. The main amelioration of the algorithm could be the upgrade of the simple projection method to a sub-set projection method using only part of the $C_N^2(h)$ profile at each iteration. These latter modification could improve the estimation of $C_N^2(h)$ profile low altitude layers. Finally, the diminution of the baseline between the two sub-aperture and the acquisition of a wider field of view camera is also considered. The combination of both baseline reduction and and field of view improvement would also give better resolution in low altitude layers.

REFERENCES

1. M. Azouit and J. Vernin, "Optical turbulence profiling with balloons relevant to astronomy and atmospheric physics.," *Publ. Astron. Soc. Pac.* **117**, pp. 536–543, 2005.
2. A. Tokovinin, V. Kornilov, N. Shatsky, and O. Voziakova, "Restoration of turbulence profile from scintillation indices," *MNRAS* **343**, pp. 891–899, 2003.
3. G. J. Lambert, "Improved detection of atmospheric turbulence with slodar," *Optics Express* **15**, pp. 14844–14860, 2007.
4. V. G. Kornilov and M. V. Kornilov, "The revision of the turbulence profiles restoration from mass scintillation indices," *Experimental Astronomy* **29**, pp. 155–176, 2011.
5. A. Ziad, J. Maire, J. Borgnino, W. D. Ali, A. Berdja, K. B. Abdallah, F. Martin, and M. Sarazin, "MOSP : Monitor of outer scale profile," in *1st AO4ELT conference*, EDP Sciences, 2010.
6. J. Maire, A. Ziad, J. Borgnino, and F. Martin, "Measurements of profiles of the wavefront outer scale using observations of the limb of the moon," *Mon. Not. R. Astron. Soc.* **377**, pp. 1236–1244, 2007.
7. M. Sarazin and F. Roddier, "The ESO differential image motion monitor," *Astron. Astrophys.* **227**, pp. 294–300, 1990.
8. R. Avila, A. Ziad, J. Borgnino, F. Martin, and A. Agabi, "Theoretical spatiotemporal analysis of angle of arrival induced by atmospheric turbulence as observed with the grating scale monitor experiment," *J. Opt. Soc. Am. A* **14**, pp. 3070–3082, 1997.
9. R. Conan, J. Borgnino, A. Ziad, and F. Martin, "Analytical solution for the covariance and for the decorrelation time of the angle of arrival of a wave front corrugated by atmospheric turbulence," *J. Opt. Soc. Am. A* **17**(10), pp. 1807 – 1818, 2000.
10. M. Bertero and P. Boccacci, *Introduction to Inverse Problems in Imaging*, CRC Press, 2010.
11. F.Roddier, "The effects of atmospheric turbulence in optical astronomy," *Progress in Optics* **19**, pp. 281–376, 1981.
12. A. Ziad, F. Blary, J. Borgnino, Y. Fanteï-Caujolle, E. Aristidi, F. Martin, H. Lantri, E. Bondoux, and D. Mekarnia, "PML/PBL: A new generalized monitor of atmospheric turbulence profiles," in *3rd AO4ELT conference*, 2013.